Synoptic-Scale Precursors of East Asia/ Pacific Teleconnection Pattern Responsible for Persistent Extreme Precipitation in the Yangtze River Valley

Yang Chen[a,b] and Panmao Zhai[b] ★

[a] Department of Atmospheric Science, Nanjing University of Information Science & Technology, Nanjing, China

[b] State Key Laboratory of Severe Weather, Chinese Academy of Meteorological Sciences, CMA, Beijing, China

★Correspondence to: P.M. Zhai, No. 46 Zhong-guan-cun-nan-da-jie, Haidian, Beijing, China. **E-mail**: pmzhai@cma.gov.cn

Accepted by *Quart. J. Roy. Meteor. Soc.*, in press

Abstract

Synoptic-scale precursors of typical East Asia/ Pacific (EAP) teleconnection pattern responsible for persistent extreme precipitation events (PEPEs) in the Yangtze River Valley (YRV) are investigated based on a composite analysis. The results reveal that about one week prior to PEPEs, a blocking high develops near the Sea of Okhotsk owing to an eastward energy dispersion and further strengthens markedly due to a poleward energy dispersion from low latitudes. Subsequently, a meridional tripole structure of typical EAP pattern becomes well established by this blocking and a westward-migrated strong negative anomaly at mid-latitudes/positive anomaly at lower latitudes. In the lower troposphere, a westward-progressive anomalous anticyclone-cyclone pair can be identified up to about a week prior to PEPEs, contributing to greatly enhanced moisture transport towards the YRV with a magnitude anomaly over 3 standard deviations above normal. A mid-latitude anomalous cyclone associated with the EAP pattern evolution and the eastward-extended South Asia High combine to provide favorable upper-level divergence. Correspondingly, strong ascent of low-level warm/moist air along a quasi-stationary front leads to PEPEs in the YRV. A contrastive analysis between evolution of typical wet and dry EAP regimes indicates that EAP-induced PEPEs are more likely to occur in the YRV with the ridge of the western Pacific subtropical high typically staying around northeastern quadrant of the South China Sea. This contrastive analysis also highlights the importance of the upstream pre-existing ridge to early strengthening of the Okhotsk blocking.

Key Words: East Asia/ Pacific teleconnection; persistent extreme precipitation; precursors

1. Introduction

Certain recurrent large-scale flow regimes have been reported to be responsible for long-lived circulation anomalies, which further result in prolonged extreme weather conditions (Dole and Gordon, 1983; Dole, 1986; Higgins and Mo, 1997; Archambault *et al.*, 2008; Lau and Weng, 2002). The duration of these regimes spans from several days to a few weeks. The teleconnection pattern is deemed to be one of such regimes. For instance, the Pacific–North American (PNA) teleconnection (Wallace and Gutzler, 1981) can substantially modulate the amount of precipitation received by the Northeastern United States in the cool-season, because the PNA phases are linked to the strength and the location of jet stream and storm track (Archambault *et al.*, 2008, 2010). Blocking episodes are another typical case of such regimes (Rex, 1950), which usually lead to anomalous storm tracks by obstructing normal eastward progressive synoptic disturbances (Carrera *et al.*, 2004).

During boreal summer, the Pacific-Japan (P-J) teleconnection has been recognized as a dominant mode over East Asia and it exerts great influences on East Asia summer monsoon (Nitta, 1987; Nitta and Hu, 1996; Huang and Sun, 1992; Huang, 2004; Lau *et al.*, 2000; Hirota and Takahash, 2012). This teleconnection pattern primarily reflects the configuration of three key systems, namely the western Pacific subtropical high (WPSH), the Mei-Yu trough and the Okhotsk high over northeast Asia (Bueh *et al.*, 2008), and it is also called East Asia/Pacific (EAP) pattern by Huang and Li (1987). The positive (negative) phase of the EAP teleconnection pattern at 500 hPa is predominately characterized by positive (negative) geopotential height anomalies around the Sea of Okhotsk and the western Pacific subtropical area respectively, sandwiching a negative (positive) height anomaly at mid-latitudes over East Asia. Hoskins and Karoly (1981) noted that Rossby waves triggered by a low-latitude source could propagate strongly poleward as well as eastward. Based on theoretical analysis and numerical experiments, both Huang (1985) and Nitta (1987) pointed out that the EAP (P-J) teleconnection was primarily triggered by anomalous convective activity near the western Pacific warm pool. Recently, Kosaka and Nakamura (2006, 2010) have revealed that this poleward dispersion mainly occur below the mid troposphere. Persistent circulation anomalies during positive (negative) EAP phases may result in cool (hot) summers in Japan and floods (droughts) in the Yangtze River in China (Nitta, 1987; Huang and Sun, 1992; Huang, 2004; Lau and Weng, 2002). Accordingly, this teleconnection pattern has been widely used in the operational prediction of climate anomalies on a seasonal timescale over East Asia (Huang, 2004). Substantial scientific attention has therefore been paid to the EAP teleconnection pattern itself and its influences on East Asian summer monsoon on interannual to inter-decadal timescales (Lau and Weng, 2002; Lau *et al.*, 2000).

Concurrently long-lived circulation anomalies from the lower to the upper troposphere are capable of inducing prolonged intense precipitation (Chen and Zhai, 2014a), referred to as persistent extreme precipitation events (PEPEs) (Chen and Zhai, 2013). Actually, regional floods tend to be induced by these PEPEs persisting for at least three consecutive days. Root *et al.* (2007) have noted that many high-impact weather events failed to be recognized in the model output by even experienced forecasters. Recognizing the potential for significant weather events based on patterns and anomalies may therefore be another available method in improving high-impact weather prediction (Grumm and Hart, 2001). Some recurrent teleconnection patterns have already served as a tool for predicting high-impact precipitation events (Archambault *et al.*, 2008, 2010; Lau and Weng, 2002). Encouragingly, the behaviors of teleconnection patterns have become predictable by forecast models up to two weeks in advance, especially during their extreme phases (Archambault *et al.*, 2010; Johansson, 2007). Specifically, EAP patterns have been frequently detected during some famous PEPEs that triggered severe flooding in the YRV. For example, PEPEs in 1991 and 1998, both of which resulted in thousands of deaths and casualties as well as billions of dollars in economic losses, have been reported to be obviously associated with the EAP pattern (Chen and Zhai, 2014a; Huang 2004). It is therefore of great practical value to quantify relationships between the EAP-related persistent circulation anomalies and extreme precipitation. Though some attention has been paid to synoptic structure of EAP (P-J) pattern recently (Bueh *et al.*, 2008; Sato and Takahashi, 2006; Ogasawara and Kawamura, 2007), the influences of EAP-related persistent anomalies on PEPEs on synoptic timescales have hitherto been rarely reported.

The main objective of this study is to investigate the influences of the EAP teleconnection pattern evolution on PEPEs in the Yangtze-River Valley (YRV, region marked by rectangle in Figure 1a) on synoptic timescales. Of particular importance is to identify synoptic precursor anomalies related to the EAP pattern evolution that are capable of inducing PEPEs in the YRV. The YRV is selected as the study area because this region is frequently affected by PEPEs associated with the stationary Mei-Yu front (Chen and Zhai, 2013, 2014a; Ding and Chan, 2005), and it is one of the most populated as well as the most economically developed regions in China. Correspondingly, PEPEs in this region represent great threats to both society and human.

2. Data and Method

2.1. Data

The data of observed daily precipitation amounts at 50 stations located in the YRV (dots in the rectangle in Figure 1a) during 1961-2010 are used to build domain-averaged precipitation events database. This data is kindly provided by the Climate Data Center (CDC) of the National Meteorological Information Center (available online http://cdc.cma.gov.cn/home.do), China Meteorological Administration (CMA).

The daily reanalysis data are provided by the National Centers for Environmental Prediction and National Center for Atmospheric Research (NCEP/NCAR), at a horizontal resolution of 2.5°×2.5° (Kalnay *et al.*, 1996). The data used in this study includes geopotential height (gpm), horizontal wind (m/s), specific humidity (kg/kg), air temperature (K), and relative humidity (%). Another reanalysis data of higher resolution, Climate Forecasting System Reanalysis (CFSR, Saha *et al.*, 2010), is also employed. Highly similar results, to be documented in the following section 4, can be achieved by using the CFSR. In order to include as many typical cases as possible (especially cases before 1979), the results based on the NCEP/NCAR reanalysis are presented, considering shorter time coverage of the CFSR. Additionally, the horizontal resolution of 2.5°×2.5° is high enough for large-scale circulation analyses.

PEPEs tend to occur in the YRV during June-July (Chen and Zhai, 2013), when is also the typical Mei-Yu episode (Ding, 1992). June and July are therefore selected as the study period.

2.2. Methods

This study is based on a composite analysis, which is a simple and effective method in identifying and typing synoptic-scale circulation patterns and their precursors associated with extreme events (Sisson and Gyakum, 2004; Grotjahn and Faure, 2008).

Anomalies of different variables, such as geopotential height and horizontal wind, tend to appear both in the lower and the upper troposphere concurrently during extreme precipitation (Graham and Grumm, 2010; Milrad *et al.*, 2010; Chen and Zhai, 2014a, b). The predictors therefore shouldn't be considered individually, because only opportune coincidences make the synoptic situations excessively dangerous (Müller *et al.*, 2009). Further, anomalies in different meteorological parameters associated with the EAP pattern evolution have also been detected both in the lower and the upper troposphere (e.g. Bueh *et al.,* 2008). Accordingly, in addition to geopotential height anomalies constituting the EAP pattern at 500 hPa, it is also necessary to take the anomalies in moisture transport in the lower troposphere and favorable divergence in the upper troposphere related to the EAP pattern or during the EAP pattern into account. These analyses will render a more systematic understanding in the mechanism of the EAP-induced PEPEs.

Composites of normalized anomalies are also performed following the method introduced by Hart and Grumm (2001). The composites of normalized anomalies are used to estimate the extremity of significant weather and how unusually large departures from normal in various meteorological parameters might be used as a tool for predicting high-impact precipitation events (Junker *et al.*, 2008). Following the method described by Hart and Grumm (2001), the normal situation here refers to a climatologic mean of related parameters evaluated via 21-day mean (from 1971-2010), centered on the day being investigated. The standard deviation is denoted by σ hereafter. Moisture flux (MF) in this study is represented as the vector composition of the product of the specific humidity and horizontal wind. The normalized anomalies of MF are evaluated by departures from the mean value of the magnitude of the total moisture flux (Junker *et al.*, 2008).

3. Identification of typical EAP regimes responsible for persistent extreme precipitation events

Initially, a normalized daily EAP index (EAPI) is calculated as follows: (1) during 1^{st} June-31^{st} July, daily normalized geopotential height anomaly at 500 hPa are calculated at each grid; (2) three points, namely WP (20°N, 120°E), EA (37.5°N, 120°E) and OK (60°N, 130°E), are selected to represent three anomaly centers in the western Pacific, mid-latitudes in East Asia, and the Sea of Okhotsk respectively during EAP regimes (Nitta, 1987; Bueh *et al.*, 2008; Hirota and Takahash, 2012); (3) the EAPI is subsequently defined as $I=1/3H_{WP}-1/3H_{EA}+1/3H_{OK}$, with H_{wp}, H_{EA}, H_{OK} representing the normalized 500 hPa geopotential height anomaly of the above three points respectively. Considering the fact that EAP-related intense precipitation occurs in the YRV during positive phases of EAP pattern (Huang, 1985; Huang, 2004), the anomalies in these three points are preliminarily required to be distributed as "+ - +".

Based on above criteria, a typical EAP regime associated with PEPEs (referred to as typical wet EAP regime) is considered when meeting the following criteria:

(1) a daily EAPI value of 1.0σ (one standard deviation) or greater persists for at least three consecutive days;

(2) normalized domain-averaged precipitation in the YRV equals to or exceeds 1.0σ in every day during EAP regimes.

One standard deviation is widely adopted as the threshold to define typical anomalous circulation regimes (Archambault *et al.*, 2008, 2010). The first criterion therefore aims to identify typical EAP regimes. The second criterion guarantees that extreme precipitation occurs simultaneously. Relaxed thresholds of both intensity and persistence are necessary for identification of combined regimes to ensure an adequate sample size (Archambault *et al.*, 2010). Considering the shorter persistence of extreme precipitation periods (Chen and Zhai, 2013), 3-day is adopted as the minimum duration. Correspondingly, persistent extreme precipitation events (PEPEs) in this study refer to the periods including at least three consecutive days with normalized daily precipitation greater than 1σ above normal. Actually, this duration mainly focuses on extreme phases of both EAP regimes and precipitation, prior to when both of them may likely be developing. Further, relatively smaller threshold of 1σ for extreme precipitation also aims to ensure the continuity and integrity of the extreme precipitation process in the YRV (Ren *et al.*, 2013). Though the relatively smaller threshold of 1σ was adopted, 75% of the identified days witnessed extreme precipitation of 2σ above normal (Figure 1b). Moreover, days with extreme precipitation of 3.5σ above normal and 5.5σ above normal account for 50% and 25% of the total identified days respectively. Such distribution of precipitation intensity indicates the extremity of the identified events and suggests the rationality of adoption of 1σ for EAP-related extreme precipitation identification. Furthermore, these events identified based on 1σ of domain-averaged series may imply 40-50mm day^{-1} or more in the precipitation center at an individual station level (see Figure 2, day 0-2). Though 40-50mm day^{-1} (day 0-2) may not be considered very extreme for an individual station in the YRV during June-July, the accumulated precipitation amount of 150-200mm or more, owing to the long duration, will likely trigger a severe flooding in the YRV within a few days. The identified events are therefore of high disaster-causing potential. To further ensure all the key systems, rather than either of them, being active enough during PEPEs, absolute values of three centers, i.e. H_{WP}, H_{EA} and H_{OK}, are required to be greater than 0.75σ in every day during PEPEs. The adoption of 0.75σ in every day for individual centers is based on considerations of their possible slight changes in both intensity and positions during PEPEs. Such combination of typical EAP regimes and concurrent extreme precipitation episodes is referred to as *typical wet EAP regimes* hereafter.

There are 20 typical wet EAP regimes identified during 1961-2010 based on above criteria, as listed in Table 1. It has to be pointed out that the EAP teleconnection represents only one of the favorable patterns responsible for such prolonged extreme precipitation events in the YRV. These 20 typical cases account for about 22% of the total PEPEs identified based on 1σ persisting for at least three consecutive days in the YRV during 1961-2010. Of particular note is that remaining 78% events are not absolutely exempt from influences of EAP patterns. It is possible that in some cases, the EAP pattern also appears over East Asia, however its intensity fails to satisfy the criterion of ‘a typical regime’, a daily EAPI value reaching 1.0σ or greater. Thus, the contribution of weak or even obscure EAP patterns in triggering PEPEs in these cases may be relatively small compared with the counterpart in the cases with typical EAP regimes. Consequently, these 20 typical cases are more suitable to investigate possible EAP-related mechanisms for PEPEs in the YRV. Further considering the complexity and diversity of underlying mechanisms responsible for PEPEs in the YRV, such as influences of upstream blocking episodes and typhoon and/or its remnants (Chen and

Zhai, 2013; Chen and Zhai, 2014a), this percentage may imply the importance of the EAP pattern in inducing PEPEs in the YRV during Mei-Yu periods.

Obviously, the typical EAP regimes is predominantly characteristic of positive height anomalies of more than 1.0σ above normal in the western Pacific and at high latitudes over East Asia simultaneously, sandwiching a negative anomaly of 3σ below normal in the immediate north of the YRV (Figure 1a). This pattern reflects the westward-extension and intensification of the WPSH and the establishment and maintenance of the Okhotsk blocking high, as well as the deepening of the Mei-Yu trough. An obvious splitting of the mid-latitude flow extends over approximately 60° of longitude (90°–150°E), resulting in a distinct equatorward shift of the main westerly flow. The duration of these significant anomalies spans from 3 days to 13 days, resulting in long-lasting extreme precipitation (Table 1).

4. Precursor and simultaneous circulation

In this section, day 0 denotes the onset (start date in Table 1) of typical EAP regimes, and day-*d* refers to the d^{th} day prior to (negative) or after (positive) the onset. Before composite, a manual inspection for every event is performed to check the similarity in circulation patterns between different events and further to achieve little smeared composites. Moreover, the principal synoptic features of the composite, to be documented in the following, are similarly presented in composites based on the subsets of 20 typical cases grouped arbitrarily (i.e., in chronological order; not shown), implying the sufficient insensitiveness of composites of the 20 typical cases to the inclusion or exclusion of specific events. Further, considering the possible high-amplitude of circulation patterns during PEPEs and resultant unequal variances of composited fields during PEPEs and climatology (Chen and Zhai, 2014a, b), both ordinary Student's *t*-test and Welch's *t*-test (Welch, 1947) are employed to achieve more rigorous statistical significance. Only the results satisfying both criteria at the 5% level at least are deemed to be statistically significant.

The temporal evolution of precipitation prior to and during typical wet EAP regimes is presented in Figure 2. Near the onset of typical wet EAP regimes (day -1, figure not shown), greatly enhanced precipitation is observed in the YRV, followed by long-lasting extreme precipitation at a regional scale during typical EAP regimes (day 0-2). Large areas under influence of extreme precipitation during day 0-2 indicate that the identified events are synoptic processes, rather than local convective events. Every individual event shares similar synoptic characters of precipitation with the composited results. The precursor features of the typical wet EAP regimes are investigated as follows:

4.1. 500 hPa geoptential height

On day -7, two ridges with height anomalies of 1σ above normal exist near the sea of Okhotsk and to the west of the Ural Mountain at mid-high latitudes, respectively (Figure 3). A broad shallow trough is sandwiched between them, providing a zonally-elongated westerly waveguide (e.g. Hoskins and Ambrizzi, 1993) for Rossby wave energy dispersion. Accordingly, a distinct energy propagation along this westerly waveguide from west of the Ural Mountain to East Asia can be clearly identified (indicated by wave flux vectors defined by Takaya and Nakamura (2001)). This zonally distributed ridge-trough-ridge wave train at mid-high latitudes is similar to the West Europe-Japan (E-J) pattern (Wakabayashi and Kawamura, 2004), and similar eastward-propagating wave energy before and during EAP regimes has also been found in some other studies (e.g. Bueh *et al.*, 2008; Sato and Takahashi, 2007). No obvious negative anomalies can be detected at mid-latitudes over East Asia on this day. From day -6 to day -3, a negative anomaly of 1σ below normal progresses westward from 170°E with little change in magnitude. By day -4, it has arrived at southern Japan. Meanwhile, the WPSH (denoted by 588dagpm-contour) keeps extending westward and reaches 120°E. During this period, the energy dispersion, persistently emanating from the ridge to the west of the Ural Mountain toward East Asia, contributes to the maintenance of the Okhotsk blocking high. The ridge in the west itself weakens a little and retrogrades southward gradually. On day -4, a poleward energy dispersion from lower latitudes in East Asia is discernible, resulting from the suppression of convective activity to the east of Philippines covered by the westward-extended WPSH (Nitta, 1987; Huang, 1985). Subsequently, the EAP-related poleward wave fluxes enhance greatly due to the further westward extension and intensification of the WPSH (day -2 to day 2). The convergence between the poleward wave fluxes and eastward wave fluxes at high latitudes strengthens the Okhotsk blocking markedly. Meanwhile, the mid-latitude trough deepens manifestly with negative anomalies of more than 2σ below normal, owing to the confluence between the poleward wave fluxes and upstream southeastward wave fluxes. By day 0, the typical EAP pattern as presented in Figure 1a becomes well established and then persists for several days.

Different from the double blocking high pattern described by Chen and Zhai (2014a), the ridge in the west is anchored to the west of the Ural Mountain rather than extends eastward. Further, it weakens and retrogrades southward rather than strengthens and extends toward high latitudes prior to the onset of PEPEs. Figure 3 clearly shows that a Ω-type blocking high (Rex, 1950) has been developing near the Sea of Okhotsk from day -7 onward, preceding the development of typical EAP pattern. This long-lived Okhotsk blocking high acts to maintain a robust meridional circulation, providing favorable conditions for the development of subsequent EAP pattern and related persistent extreme precipitation. The strengthening Okhotsk blocking high displaces the main westerly flow much equatorward by day -2. Northwesterlies therefore prevail in the upstream of the YRV, steering the cold/dry air required by the frontogenesis into the YRV. The confluence between cold/dry air and warm/moist air conveyed by the westward-shifted WPSH enhances the gradients of both temperature and specific humidity around the YRV, which favors the formation the Mei-Yu front (Ninomiya and Shibagaki, 2007). Additionally, eastward-propagating short-wave troughs tend to be blocked by the Okhotsk blocking high and then they are steered into the YRV by the resultant equatorward westerlies (Ding and Reiter, 1982). Consequently, local rainfall is further enhanced (Samel *et al.*, 1999, 2003).

4.2. Lower-level wind and water vapor transport

At 850 hPa (Figure 4), an anomalous anticyclone originated from the east of 150°E begins to migrate westward from day -6 onward, followed by a westward-progressive anomalous cyclone at mid-latitudes from day -5 onward. Both of them strengthen during westward migration. By day -4, the west boundary of the anomalous anticyclone has arrived at 120°E, with an enhanced moisture flux (MF) of a magnitude anomaly over 1.5σ above normal to its northern flank. Subsequently, a strengthening anticyclone-deepening cyclone pair prevails at mid-latitudes over East Asia, contributing to a greatly enhanced moisture flux with a MF magnitude anomaly of 3σ above normal. The confluence between the northerlies steered by the anomalous cyclone and southwesterlies to the northern flank of the anticyclone maximizes the moisture convergence in the immediate south of the YRV (blue contours). Obviously, the anomalously abundant moisture necessary for PEPEs is primarily transported by the anomalous anticyclone related to the westward-extended WPSH, rather than by the southwesterly originated from the Bay of Bengal (Qian *et al.*, 2004). During typical EAP regimes (day 0 to day 2), a strong moisture convergence exists between the anomalous anticyclone and cyclone with a MF anomaly over 3.5σ above normal. Of particular note is that the zonally westward progression of the anomalous anticyclone, instead of the northwest migration as previously reported (Mao *et al.*, 2010; Yang *et al.*, 2010), is markedly observed prior to the establishment of typical EAP regimes. In addition, an anomalously deepening cyclone, rather than a dissipating one as reported by Mao *et al.* (2010), is observed in the YRV.

4.3. Upper-level divergence

The temporal evolution of the typical wet EAP pattern in the upper troposphere (200 hPa) is similar to that at 500 hPa especially at mid-high latitudes (Figure 5), indicating an equivalent barotropic structure of EAP pattern at mid-high latitudes (Hoskins and Karoly, 1981; Tsuyuki and Kurihara, 1989). The negative anomaly at mid-latitude can reach 3σ below normal during typical EAP regimes (day 0-2). Accompanying developing of the EAP-related negative anomaly at mid-latitude, the westerly jet displaces equatorward gradually (bold green lines) and is finally anchored in the region immediate north of the YRV eastward to Japan. Accordingly, the YRV is well located beneath the southern section of westerly jet. Furthermore, the deepening of the mid-latitude anomalous cyclone render a sharper meridional height gradient from the YRV to Japan, contributing to a further accelerating westerly jet (shadings in Figure 5). Also evident is the eastward extension of the South Asia High (SAH, indicated by the 12520gpm contour, black solid line), so northerly flows prevail above upstream of the YRV (vectors). The mid-latitude anomalous cyclone embedded in these northerly flows favor advection of positive vorticity toward immediate north of the YRV. The extra positive vorticity triggers upper-level divergence (Holton, 2004), which facilitates development and maintenance of strong ascent during the persistence of extreme precipitation in the YRV.

At the upper troposphere, in addition to the distinct EAP pattern, another wave train at mid-latitudes seems to propagate slowly along the Asian Jet, and it is called the Silk Road pattern (Kosaka *et al.,* 2009) or West Asia-Japan pattern (Wakabayashi and Kawamura, 2004). Simultaneous existence of two wave trains at mid-latitudes and high-latitudes may be attributed to the European blocking high, which excites eastward-propagating wave activity fluxes at high-latitudes and southeastward-propagating wave activity fluxes reaching mid-latitudes (Iwao and Takahashi, 2008).

4.4. Vertical structure of the quasi-stationary front related to typical wet EAP pattern

Considering the fact that the Mei-Yu front is characterized by a relatively weak temperature contrast and a sharp moisture contrast, equivalent potential temperature (θ_e) rather than potential temperature is therefore widely employed to depict the Mei-Yu front (Ding, 1992; Zhou *et al.*, 2004; Lai *et al.*, 2011). The moist air denoted by high specific humidity in the lower troposphere corresponds well to large θ_e (Figure 6), indicating that moisture rather than temperature dominates the equivalent potential temperature signature. From day -4 onward, the low-level southerlies originated from low-latitudes (15°N) become more organized, primarily owing to the arrival of the WPSH at 120°E. Subsequently, further westward extension and enhancement of the WPSH (Figure 3 and Figure 4) contribute to the acceleration of these low-level southerlies. Meanwhile, the northerlies from mid latitudes steered by the deepening trough prevail in the mid-upper troposphere. Correspondingly, a pronounced southward-intrusion of the cold/dry air can be observed in the mid-upper levels. By day -1, obvious descending northerlies are detected over 35°-45°N, where is well located in the rear flank of the upper-level trough. This descent is consistent with the forcing of anticyclonic vorticity advection behind the trough (Holton, 2004). Also obvious is a thicker and moister layer (indicated both by 355K contour and shading specific humidity) in the lower troposphere well over the YRV from day -2 onward, providing a more unstable condition necessary for extreme precipitation. Convergence between the ascending low-level warm/moist southerlies and the descending upper-level cold/dry northerlies result in a greatly enhanced θ_e gradient in the northern YRV (dense contours) by day 0, indicating the formation of a typical Mei-Yu front (Ding, 1992). Persistent strong ascent of low-level warm/moist southerlies along this quasi-stationary front can be clearly identified within the YRV (day 0 to day 2), contributing to the persistent extreme precipitation. What is worth mentioning is that once extreme precipitation related to quasi-stationary front initiates, resultant diabatic heating would also exert some influences of surrounding circulations. Such feedback may be a contributing factor in maintaining local circulation anomalies, which in turn lead to a longer duration of extreme precipitation (Lu and Lin, 2009).

4.5. Contrastive analyses

A question of whether these long-lived anomalies during typical EAP regimes will definitely lead to PEPEs in the YRV is likely to be raised naturally. The answer to this question will provide a more in-depth understanding in underlying mechanism of PEPEs related to the EAP pattern. To this end, some additional cases are selected for comparison by demanding that during typical EAP regimes defined as same as the first criterion in section 3, the normalized domain-averaged daily precipitation in the YRV on the same day is smaller than -1σ. Also, absolute values of three centers are required to be greater than 0.75σ in every day during PEPEs. These criteria succeed to identify typical EAP regimes that can't result in PEPEs in the YRV (Table 2; Figure 7b). This kind of typical EAP pattern is hereafter referred to as *typical dry EAP regime*. Of particular note is that the typical dry EAP regimes differ from the above wet regimes only in concurrent occurrence of extreme precipitation, not representing negative phases of the EAP pattern.

The comparison reveals that the most obvious differences during dry EAP pattern and wet EAP pattern lie in the meridional location of the WPSH and strength of the Okhotsk blocking high (Figure 7a). Though the WPSH also extends to the west of 120 °E during typical dry EAP regimes, it displaces more to the south compared with that during typical wet EAP regimes, with its ridge anchored near 15 °N. The moist air is therefore less likely conveyed to the YRV, leading to less precipitation relative to climatology (Figure 7b). Meanwhile, a weaker Okhotsk blocking high is observed during typical dry EAP regimes (shadings in Figure 7a). Prior to the onset of typical dry EAP regimes, due to the absence of the positive anomalies to the west of the Ural Mountain (green hatched lines to the west of 60 ° E in Figure 8), the zonal wave activity fluxes are weak and are not as well-organized as those in typical wet EAP regimes situation (Figure 8). The Okhotsk blocking high correspondingly develops slowly and is not well-established until day -1, mainly resulting from the EAP-related poleward energy dispersion from low latitudes. Also, the weaker Okhotsk blocking high may be possibly associated with absence of transient eddies (Nakamura and Fukamachi, 2004). Interestingly, no significant differences are found in the region of western positive anomalies during dry and wet EAP regimes (Figure 8, day 0-2). This phenomenon suggests that the western ridge is important to the early strengthening of the Okhotsk blocking high, while the EAP-related meridional energy dispersion is the key factor in maintaining the Okhotsk blocking high and resultant meridional circulation pattern. Another obvious difference is that the WPSH extends westward much slower prior to the onset of the dry EAP pattern, reaching 120°E by day -1. In the lower troposphere (Figure 9), an anomalous cyclone is anchored in the northern South China Sea from day -8 to day -3, advecting abundant moisture toward east and northeast of the Philippines. This anomalous cyclone directly prevents the westward extension of the WPSH. From day -2 onward, the anomalous cyclone dissipates, and then is replaced by an anomalous anticyclone, which is much weaker and displaces more to the south compared to the counterpart during typical wet EAP regimes. Correspondingly, the anomalous water vapor can only be transported to coastal region of South China (Figure 9, day 0-2). Hence, though the cold/dry air can still be steered into the YRV by the mid-latitude trough during typical dry EAP regime (Figure 9, day 0-2; Figure 10, day 2), moisture convergence fails to form in the YRV without necessary warm/moist air because of the southward displacement of the WPSH. The thick moist and warm layer is also beyond the YRV (Figure 10). Additionally, the accelerated and well-organized low-level southerlies are hardly detected prior to the onset of the dry EAP pattern. Consequently, obviously enhanced θ_e gradient doesn't appear during typical dry EAP regimes, indicating the failure of establishment of the stationary front responsible for the PEPEs in the YRV (Figure 10, comparing day 0-2 with day -8- -2). Additionally, no obvious eastward extension of the SAH is observed prior to typical dry EAP regimes (Figure not shown). Hence, the strong ascent in the YRV along the stationary front is absent during typical dry EAP regimes. So it is reasonable to conclude that the position of the WPSH is critical to EAP patterns in triggering and maintaining PEPEs in the YRV.

5. Conclusions and discussions

Based on a composite analysis, the synoptic-scale evolution of typical East Asia/Pacific (EAP) teleconnection pattern responsible for persistent extreme precipitation events (PEPEs) in the Yangtze River Valley (YRV) is investigated (referred to as *typical wet EAP pattern*). Potentials of key components in the EAP pattern for predicting PEPEs are also evaluated via composites of their normalized anomalies. Another kind of typical EAP pattern that cannot result in PEPEs in the YRV (referred to as *typical dry EAP pattern*) is analyzed as a comparison to further highlight the roles of key elements in the evolvement of the typical EAP pattern and related PEPEs. The main conclusions are summarized in a schematic (Figure 11) and stated as follows:

About one week prior to the onset of typical wet EAP pattern, a blocking develops near the Sea of Okhotsk, resulting from the upstream wave energy dispersion emanating from the positive anomaly to the west of the Ural Mountains (Figure 11b). Simultaneously, this western positive anomaly weakens and retrogrades southeastward gradually. A negative anomaly originated from about 170 °E progresses westward and arrives at southern Japan by day -4. In the meantime, the west boundary of the WPSH reaches 120 °E. By day -2, convergence between EAP-related poleward propagating wave fluxes from lower latitudes and the eastward propagating wave fluxes at high latitudes greatly strengthen the Okhotsk blocking high. The mid-latitude trough deepens manifestly with anomalies of more than 2.5 standard deviations below normal, owing to the confluence between the EAP-related poleward wave fluxes and the upstream southeastward wave fluxes. Subsequently, a well-established EAP pattern persists for several days over East Asia.

In the lower troposphere, a strengthening anomalous anticyclone/ a deepening anomalous cyclone pair progresses westward since day -6 and finally stays quasi-stationary at lower-mid latitudes over East Asia (Figure 11c). An anomalously enhanced moisture flux with a magnitude anomaly of 3σ above normal prevails to the northern flank of the anomalous anticyclone. Corresponding warm/moist air strongly converges with cold/dry air steered by the anomalous cyclone in the YRV. In the upper troposphere, a deepening mid-latitude cyclone (2.5σ below normal) and the eastward-extended the South Asia High combine to provide conductive divergence for the persistence of the extreme precipitation in the YRV (Figure 11a).

By day -4, well-organized low-level southerlies are observed from low latitudes (15°N) northward to the YRV. Subsequently, the low-level warm/moist air is elevated by the descending northerlies over 35°-45°N. Continuous confluence between these ascending warm/moist southerlies and descending cold/dry northerlies renders steep meridional gradients of both temperature and humidity, further contributing to the formation of a quasi-stationary Mei-Yu front in the northern YRV (Figure 11c). Persistent strong ascent of low-level warm/moist southerlies along this quasi-stationary front ultimately contributes to PEPEs in the YRV.

The location of the WPSH is critical in triggering and maintaining extreme precipitation in the YRV during typical EAP regimes, because it determines water vapor transport towards the YRV. The ridge of the WPSH during typical wet EAP regimes tends to be anchored around northeast quadrant of the South China Sea (22°N). During typical dry EAP regimes, though the WPSH also extends to the west of 120°E and the meridional tripole structure can also be evidently identified over East Asia, the ridge of the WPSH typically stays near 15°N, failing to transport required moisture towards the YRV. This kind of EAP pattern therefore cannot result in PEPEs in the YRV. Also in the mid-upper troposphere, the upstream effect of the positive anomaly to the west of the Ural Mountain seems important in determining early strengthening of the Okhotsk blocking high. The absence of this western ridge weakens the eastward energy dispersion, resulting in a much weaker Okhotsk blocking high during typical dry EAP regimes. In the lower troposphere, a pre-existing anomalous cyclone around the South China Sea prevents the early westward extension of the WPSH prior to typical dry EAP regimes, delaying the arrival of the WPSH at 120 °E.

Of particular note is that the applicability of the precursors identified based on the events during 1961-2010 needs to be further justified by large number of future cases after 2010. Encouragingly, similar evolution of typical EAP pattern can be obviously recognized prior to PEPEs that occurred in mid-low reaches of the YRV during 10^{th}-13^{rd} July 2012, with maximum accumulated precipitation of 350mm during four days (figure not shown).

Though the diagnoses of wave activity fluxes imply dynamical links between the three key systems, deeper investigations via numerical model simulations are still needed to justify that these concurrent anomalies share common dynamical mechanisms rather than just occur by chance. In addition, the mechanisms for the westward migration of anomalies, especially at lower-mid latitudes, will be further investigated and presented in a future study. It is also worth mentioning that most dry events listed in Table 2 occurred in early Mei-Yu period, while most wet events listed in Table 1 occurred after mid-June. This may imply that identified EAP-based precursors are of more indicative significance to occurrences of PEPEs in the YRV after mid-June.

Given that global forecast models exhibit great skills in predicting large-scale circulation evolution at lead times of 1-2 weeks, the conclusions and schematics (Figure 11) in this study may allow local forecasters to improve the prediction of high-impact precipitation by recognizing evolution of typical EAP patterns.

Acknowledgements

This study was supported by the National Key Basic Research Program of China (Grant No. 2012CB417205). Authors are grateful to Editors and two anonymous reviewers for their invaluable and constructive suggestions and comments that helped greatly improve the manuscript.

References

Archambault HM, Keyser D, Bosart LF. 2010. Relationships between large-scale regime transitions and major cool-season precipitation events in the northeastern United States. *Mon. Weather Rev.* **138**: 3454-3473.

Archambault HM, Bosart LF, Keyser D, Aiyyer AR. 2008. Influence of large-scale flow regimes on cool-season precipitation in the northeastern United States. *Mon. Weather Rev.* **136**: 2945-2963.

Bueh C, Shi N, Ji L, Wei J, Tao S. 2008. Features of the EAP events on the medium-range evolution process and the mid- and high-latitude Rossby wave activities during the Meiyu period. *Chinese Sci. Bull.* **53**: 610–623.

Carrera M, Higgins R, Kousky V. 2004. Downstream weather impacts associated with atmospheric blocking over the northeast Pacific. *J. Climate* **17**: 4823-4839.

Chen Y, Zhai PM. 2013. Persistent extreme precipitation events in China during 1951-2010. *Climate Res.* **57**: 143-155.

Chen Y, Zhai PM. 2014a. Two types of typical circulation patterns for the persistent extreme precipitation in Central-Eastern China. Quart. *J. Roy. Meteor. Soc.* doi: 10.1002/qj.2231, in press.

Chen Y, Zhai PM. 2014b. Precursor circulation features for persistent extreme precipitation in Central-Eastern China. *Weather and Forecasting* doi:10.1175/WAF-D-13-00065.1, in press.

Ding YH, Reiter RE. 1982. A relationship between planetary waves and persistent rain and thunderstorms in China. *Arch. Met. Geoph. Biocl., Ser. B* **31**: 221-252.

Ding Y. 1992. Summer monsoon rainfalls in China. *J. Meteor. Soc. Japan* **70**: 397-421.

Ding YH, Chan JCL. 2005. The East Asian summer monsoon: An overview. *Meteor. Atmos. Phys*. **89**: 177–142.

Dole RM, Gordon ND. 1983. Persistent anomalies of the Northern Hemisphere wintertime circulation: geographical distribution and regional persistence characteristics. *Mon. Weather. Rev.* **111**: 1567–1586.

Dole, RM. 1986. Persistent anomalies of the extratropical Northern Hemisphere wintertime circulation: Structure. *Mon. Weather Rev.* **114**: 178-207.

Graham RA, Grumm RH. 2010. Utilizing normalized anomalies to assess synoptic-scale weather events in the western United States. *Weather and Forecasting* **25**: 428-445.

Grotjahn R, Faure G. 2008. Composite Predictor Maps of Extraordinary Weather Events in the Sacramento, California, Region*. *Weather and Forecasting* **23**: 313-335.

Grumm RH, Hart R. 2001. Standardized anomalies applied to significant cold season weather events: Preliminary findings. *Weather and Forecasting* **16**: 736-754.

Hart RE, Grumm RH. 2001. Using normalized climatological anomalies to rank synoptic-scale events objectively. *Mon. Weather Rev.* **129**: 2426-2442.

Higgins RW, Mo KC. 1997. Persistent North Pacific circulation anomalies and the tropical intraseasonal oscillation. *J. Climate* **10**: 223-244.

Hirota N, Takahashi M. 2012. A tripolar pattern as an internal mode of the East Asian summer monsoon. *Climate Dyn.* **39(9-10)**: 2219-2238.

Holton JR. 2004. *An introduction to dynamic meteorology*. Academic press, 4th edition.

Hoskins BJ, Karoly DJ. 1981. The steady linear response of a spherical atmosphere to thermal and orographic forcing. *J. Atmos. Sci.* **38**: 1179-1196.

Hoskins BJ, Ambrizzi T. 1993. Rossby wave propagation on a realistic longitudinally varying flow. *J. Atmos. Sci.* **50**: 1661-1671.

Huang G. 2004. An index measuring the interannual variation of the East Asian summer monsoon—The EAP index. *Adv. Atmos. Sci.* **21**: 41-52.

Huang RH. 1985. The numerical simulation of the three-dimensional teleconnections in the summer circulation over the Northern Hemisphere. *Adv. Atmos. Sci.* **2**: 81-92.

Huang R, Li W. 1987. Influence of the heat source anomaly over the tropical western Pacific on the subtropical high over East Asia. Proc. *International conference on the general circulation of East Asia*.

Huang R, Sun F. 1992. Impacts of the tropical western Pacific on the East Asian summer monsoon. *J. Meteor. Soc. Japan* **70**: 243-256.

Iwao K, Takahashi M. 2008. A precipitation seesaw mode between Northeast Asia and Siberia in summer caused by Rossby waves over the Eurasian continent. *J. Climate* **21**: 2401-2419.

Johansson Å. 2007. Prediction skill of the NAO and PNA from daily to seasonal time scales. *J. Climate* **20**: 1957-1975.

Junker NW, Grumm RH, Hart R, Bosart LF, Bell KM, Pereira FJ. 2008. Use of normalized anomaly fields to anticipate extreme rainfall in the mountains of northern

California. *Weather and Forecasting* **23**: 336-356.

Kalnay E, Coauthors. 1996. The NCEP/NCAR 40-year reanalysis project. *Bull. Amer. Meteor. Soc.* **77**: 437-471.

Kosaka Y, Nakamura H. 2006. Structure and dynamics of the summertime Pacific–Japan teleconnection pattern. *Quart. J. Roy. Meteor. Soc.* **132**: 2009-2030.

Kosaka Y, Nakamura M, Watanabe M, Kimoto M. 2009. Analysis on the dynamics of a wave-like teleconnection pattern along the summertime Asian jet based on a reanalysis dateset and climate model simulations. *J. Meteor. Soc. Japan* **87**: 561-580.

Kosaka Y, Nakamura H. 2010. Mechanisms of meridional teleconnection observed between a summer monsoon system and a subtropical anticyclone. part I: the Pacific-Japan pattern. *J. Climate* **23**: 5085-5108.

Lai HW, Davis CA, Jong-Dao Jou B. 2011. A subtropical oceanic mesoscale convective vortex observed during SoWMEX/TiMREX. *Mon. Weather Rev.* **139**: 2367-2385.

Lau, KM, Weng H. 2002. Recurrent teleconnection patterns linking summertime precipitation variability over East Asia and North America. *J. Meteor. Soc. Japan, Ser. II* **80**: 1309-1324.

Lau K, Kim K, Yang S. 2000. Dynamical and boundary forcing characteristics of regional components of the Asian summer monsoon. *J. Climate* **13**: 2461-2482.

Lu R, Lin Z. 2009. Role of subtropical precipitation anomalies in maintaining the summertime meridional teleconnection over the western North Pacific and East Asia. *J. Climate* **22**: 2058-2072.

Mao J, Sun Z, Wu G. 2010. 20–50-day oscillation of summer Yangtze rainfall in response to intraseasonal variations in the subtropical high over the western North Pacific and South China Sea. *Climate Dyn.* **34**: 747-761.

Milrad SM, Atallah EH, Gyakum JR. 2010. Synoptic Typing of Extreme Cool-Season Precipitation Events at St. John's, Newfoundland, 1979-2005. *Weather and Forecasting* **25**: 562-586.

Müller M, Kašpar M, Řezáčová D, Sokol Z. 2009. Extremeness of meteorological variables as an indicator of extreme precipitation events. *Atmospheric Res.* **92**: 308-317.

Nakamura H, Fukamachi T. 2004. Evolution and dynamics of summertime blocking over the Far East and the associated surface Okhotsk high. Quart. *J. Roy. Meteor. Soc.* **130**: 1213-1233.

Ninomiya K, Shibagaki Y. 2007. Multi-scale features of the Meiyu-Baiu front and associated precipitation systems. *J. Meteor. Soc. Japan, Ser. II* **85**: 103-122.

Nitta T. 1987. Convective activities in the tropical western Pacific and their impact on the Northern Hemisphere summer circulation. *J. Meteor. Soc. Japan* **65**: 373-390.

Nitta T, Hu ZZ. 1996. Summer Climate Variability in China and Its Association with. *J. Meteor. Soc. Japan* **74**: 425-445.

Qian JH, Tao WK, Lau K. 2004. Mechanisms for torrential rain associated with the Mei-yu development during SCSMEX 1998. *Mon. Weather Rev.* **132**: 3-27.

Ren X, Yang XQ, Sun X. 2013. Zonal Oscillation of Western Pacific Subtropical High and Subseasonal SST Variations during Yangtze Persistent Heavy Rainfall Events. *J. Climate* **26**: 8929-8946.

Rex DF. 1950. Blocking action in the middle troposphere and its effect upon regional climate. *Tellus* **2**: 275-301.

Root B, Knight P, Young G, Greybush S., Grumm R, Holmes R, Ross J. 2007. A fingerprinting technique for major weather events. *J. Appl. Meteor. Climatol.* **46**:1053-1066.

Saha, S, Coauthors. 2010. The NCEP Climate Forecast System Reanalysis. *Bull. Amer. Meteor. Soc.* **91**: 1015–1057.

Samel AN, Liang XZ. 2003. Understanding relationships between the 1998 Yangtze River flood and north-east Eurasian blocking. *Clim. Res.* **23**: 149-158.

Samel AN, Wang WC, Liang XZ. 1999. The monsoon rainband over China and relationships with the Eurasian circulation. *J. Climate* **12**: 115-131.

Sato N, Takahashi M. 2006. Dynamical processes related to the appearance of quasi-stationary waves on the subtropical jet in the midsummer Northern Hemisphere. *J. Climate* **19**: 1531-1544.

Sato N, Takahashi M. 2007. Dynamical processes related to the appearance of the Okhotsk high during early midsummer. *J. Climate* **20**: 4982-4994.

Sisson PA, Gyakum JR. 2004. Synoptic-scale precursors to significant cold-season precipitation events in Burlington, Vermont. *Weather and Forecasting* **19**: 841-854.

Takaya K, Nakamura H. 2001. A formulation of a phase-independent wave-activity flux for stationary and migratory quasigeostrophic eddies on a zonally varying basic flow. *J. Atmos. Sci.* **58**: 608-627.

Tsuyuki T, Kurihara K. 1989. Impact of convective activity in the western tropical Pacific on the East Asian summer circulation. *J. Meteor. Soc. Japan* **67**: 231-247.

Wallace JM, Gutzler DS. 1981. Téléconnexions in the geopotential height field during the Northern Hemisphere winter. *Mon. Weather Rev.* **109**: 784-812.

Wakabayashi S, Kawamura R. 2004. Extraction of major teleconnection patterns possibly associated with anomalous summer climate in Japan. *J. Meteor. Soc. Japan* **82**: 1577–1588.

Welch BL. 1947. The generalization of ‘‘Student’s’’ problem when several different population variances are involved. *Biometrika* **34**: 28–35.

Yang J, Wang B, Bao Q. 2010. Biweekly and 21-30-day variations of the subtropical summer monsoon rainfall over the Lower Reach of the Yangtze River Basin. *J. Climate* **23**: 1146-1159.

Zhou Y, Gao S, Shen SS. 2004. A diagnostic study of formation and structures of the Meiyu front system over East Asia. *J. Meteor. Soc. Japan, Ser. II* **82**. 1565-1576.

Table 1. The 20 typical East Asia/Pacific (EAP) teleconnection regimes responsible for persistent extreme precipitation (typical wet EAP regimes) in the Yangtze River Valley (YRV) during 1961-2010.

Year	Start Date (Day-Month)	End Date (Day-Month)	Average normalized precipitation	Average EAPI	Average H_{WP}	Average H_{EA}	Average H_{OK}
1968	4 Jul	10 Jul	2.33	1.27	1.09	-1.59	1.14
1969	11 Jul	16 Jul	4.16	1.77	1.29	-3.15	0.90
1970	10 Jul	19 Jul	3.27	2.38	1.31	-3.38	2.46
1974	14 Jul	17 Jul	4.34	1.75	0.95	-2.14	2.17
1975	26 Jun	28 Jun	3.32	1.53	1.08	-2.04	1.47
1982	17 Jul	24 Jul	3.47	1.77	1.97	-1.61	1.73
1983	5 Jul	7 Jul	3.75	1.28	1.59	-1.33	0.92
1986	4 Jul	6 Jul	2.26	1.58	0.96	-1.42	2.37
1989	15 Jun	18 Jun	4.70	1.99	1.13	-2.65	2.19
1989	29 Jun	2 Jul	2.01	1.37	0.93	-1.97	1.22
1991	1 Jul	9 Jul	3.51	1.89	2.23	-1.33	2.09
1993	23 Jul	27 Jul	1.51	1.96	1.47	-2.33	1.72
1995	21 Jun	3 Jul	3.17	2.37	1.66	-2.94	2.56
1996	29 Jun	1 Jul	4.12	1.83	2.40	-2.14	0.98
1998	16 Jun	19 Jun	4.94	2.35	1.96	-1.90	3.18
1998	20 Jul	24 Jul	5.79	2.06	1.28	-2.30	2.58
1999	15 Jul	18 Jul	1.80	1.81	1.08	-1.62	2.74
2000	8 Jun	10 Jun	4.85	1.62	1.17	-2.45	1.34
2009	29 Jun	1 Jul	4.97	2.33	1.62	-2.89	2.49
2009	22 Jul	30 Jul	3.64	1.83	1.22	-3.11	1.38

Note: the last four columns offer average index values of EAP and three centers constituting the EAP pattern, namely WP (20°N, 120°E), EA (37.5°N, 120°E) and OK (60°N, 130°E).

Table 2. The 11 typical East Asia/Pacific (EAP) teleconnection regimes during 1961-2010 that can't result in persistent extreme precipitation (typical dry EAP regimes) in the Yangtze River Valley (YRV).

Year	Start Date (Day-Month)	End Date (Day-Month)	Average normalized precipitation	Average EAPI	Average H_{WP}	Average H_{EA}	Average H_{OK}
1966	3 Jun	6 Jun	-2.45	2.41	2.21	-3.56	1.46
1967	1 Jul	3 Jul	-1.27	1.48	1.43	-2.22	0.79
1973	20 Jul	22 Jul	-1.47	1.75	0.91	-2.00	2.34
1990	15 Jul	17 Jul	-2.08	1.47	1.36	-2.10	0.97
1997	2 Jun	4 Jun	-1.82	1.55	1.27	-1.94	1.37
1998	3 Jun	5 Jun	-2.44	1.82	1.36	-2.87	1.16
2002	11 Jun	14 Jun	-2.62	2.05	1.06	-3.43	1.65
2003	12 Jun	14 Jun	-2.43	2.71	1.08	-5.28	1.76
2004	4 Jul	10 Jul	-1.45	1.71	1.15	-2.43	2.06
2005	8 Jul	10 Jul	-1.22	1.62	2.56	-1.00	1.18
2009	11 Jun	13 Jun	-2.99	1.90	1.07	-2.21	2.42

Note: the last four columns offer average index values of EAP and three centers constituting the EAP pattern, namely WP (20°N, 120°E), EA (37.5°N, 120°E) and OK (60°N, 130°E).

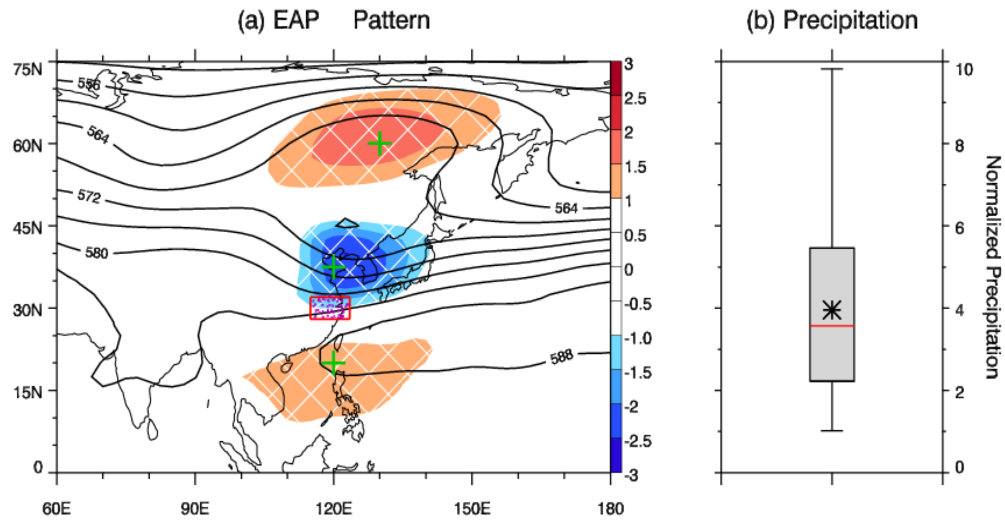

Figure 1. The circulation pattern and precipitation distribution during typical EAP regimes responsible for persistent extreme precipitation events (typical wet EAP regimes) in the YRV. a) shows the composited 500 hPa geopotential height (contour, every 4 dagpm) and composited normalized height anomalies (shading, every 0.5 standard deviation). Three green crosses represent three anomaly centers in the western Pacific, the mid-latitudes in East Asia, and the Sea of Okhotsk respectively. The hatched lines filled in the shadings indicate their significance at the 0.05 level at least. The study area, Yangtze River Valley (28-32 °N, 115-123.5 °E) is marked by red rectangle in a, with purple dots indicating meteorological stations. b) displays the box plot of normalized precipitation anomalies (right y-axis) of 110 days accumulated by all the identified cases, in which five horizontal bars indicate the minimum, first quartile, median, third quartile and the maximum respectively. The asterisk denotes the mean value.

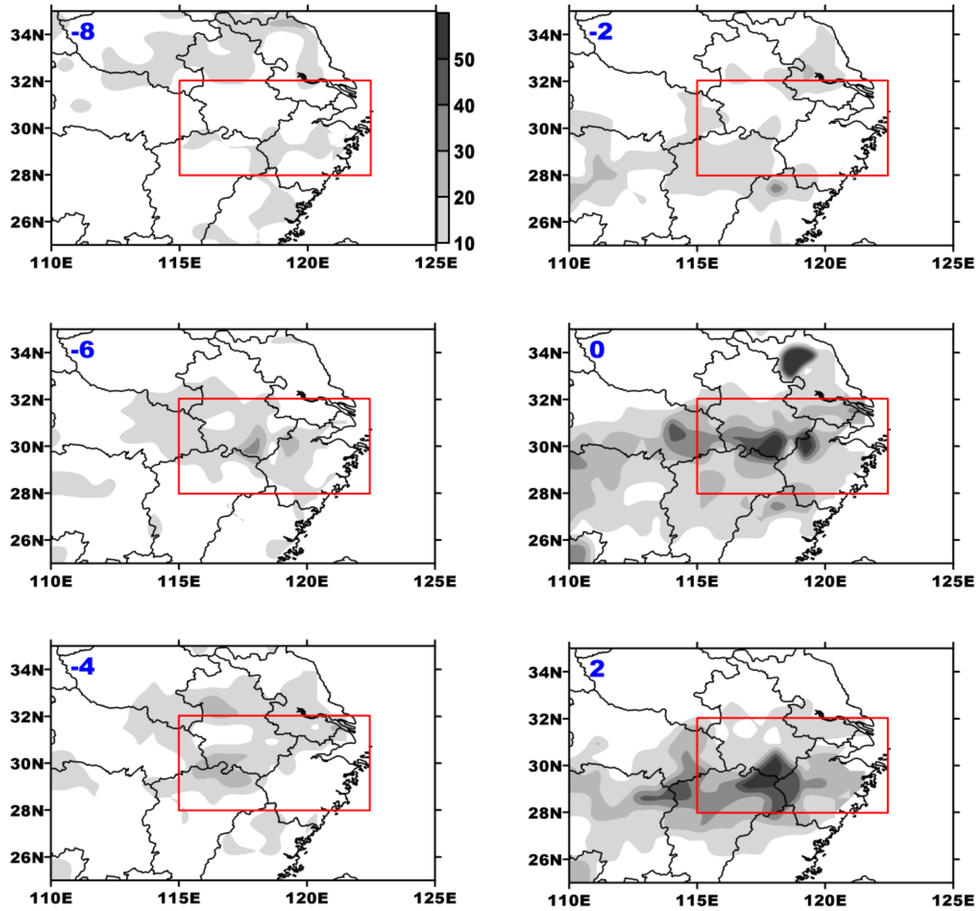

Figure 2. Composited temporal evolution of precipitation (unit: mm) in the YRV. The number-d at the upper-left corner in each panel refers to the d$^{\text{th}}$ day prior (negative) to and after (positive) the occurrence of PEPEs. Only the regions with precipitation amount of greater than 10mm are shaded, with shading interval of 10mm. The YRV is highlighted by the red rectangle.

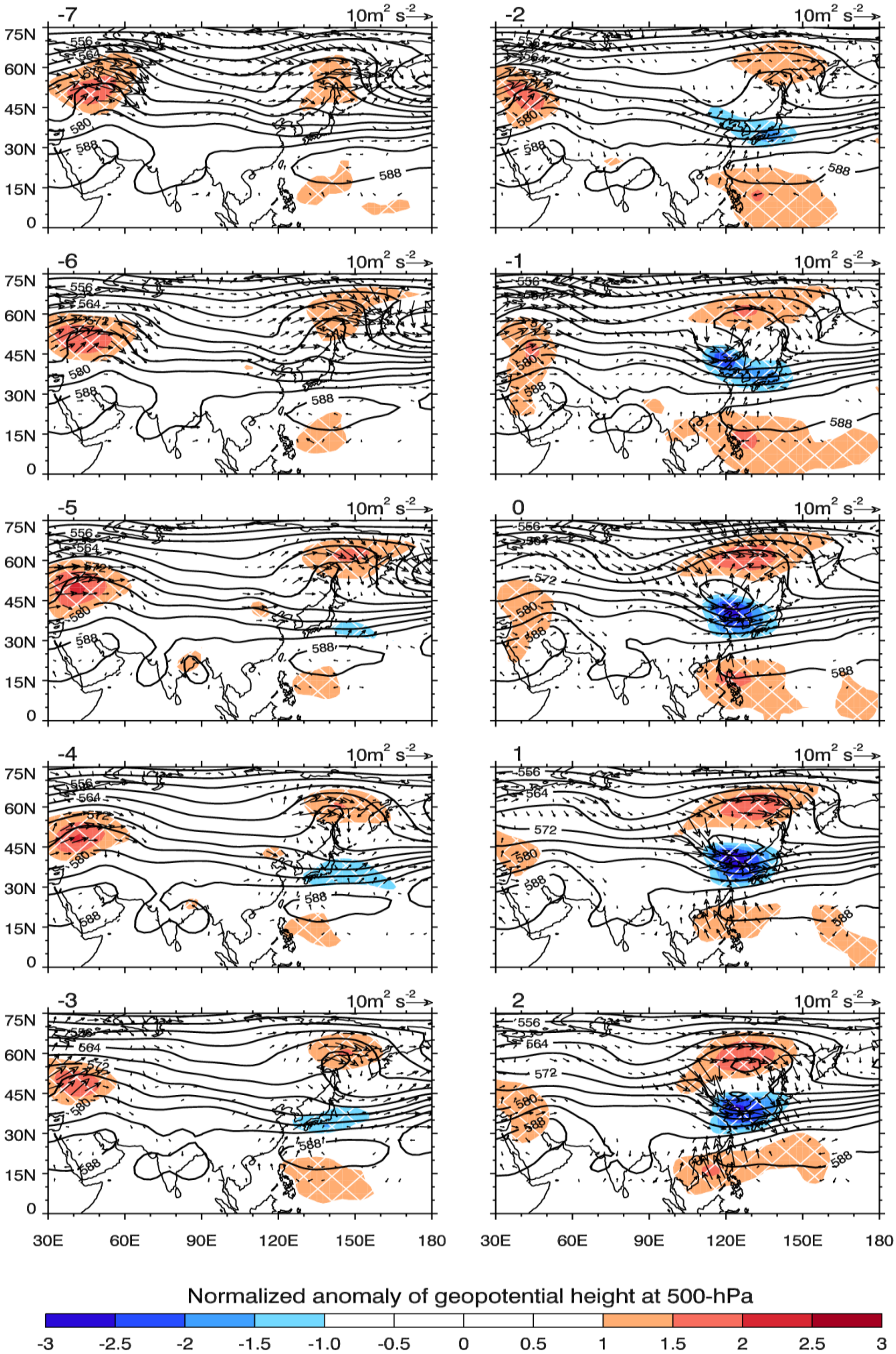

Figure 3. Composited 500 hPa geopotential height (contour, every 4 dagpm) and normalized height anomalies (shading, every 0.5 standard deviation). The vectors indicate wave activity flux (unit: m^2 s^{-2})

defined by *Takaya and Nakamura* (2001). The number above each panel represents the same meaning of that in Figure 2. And the cross-hatched shadings represent the same meaning of that in Figure 1.

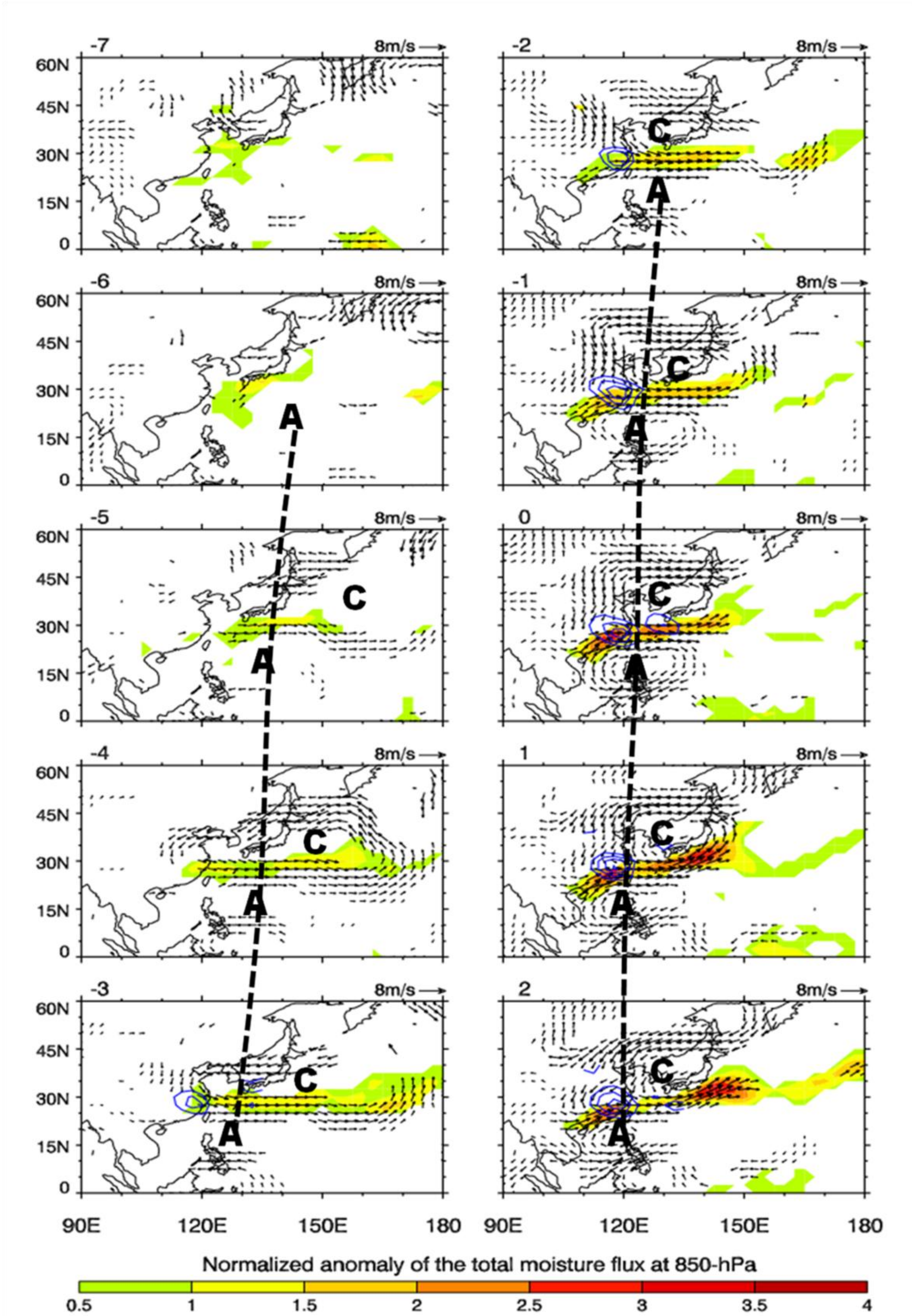

Figure 4. Composited 850 hPa horizontal wind anomaly (vectors, m/s) and normalized anomaly of total moisture flux magnitude (shadings). Only the vectors that are at least significant at the 0.05 level

are shown. The number above each panel represents the same meaning of that in Figure 2. The shading interval is 0.5σ. Blue contours of value spanning -2 to -8 with interval of -2 (unit: 10^{-8} s^{-1}), indicate moisture flux convergence. The letter 'A' and 'C' represent anomalous anticyclone and cyclone, respectively. The black dashed lines portray the westward propagation of the anomalous anticyclone/cyclone

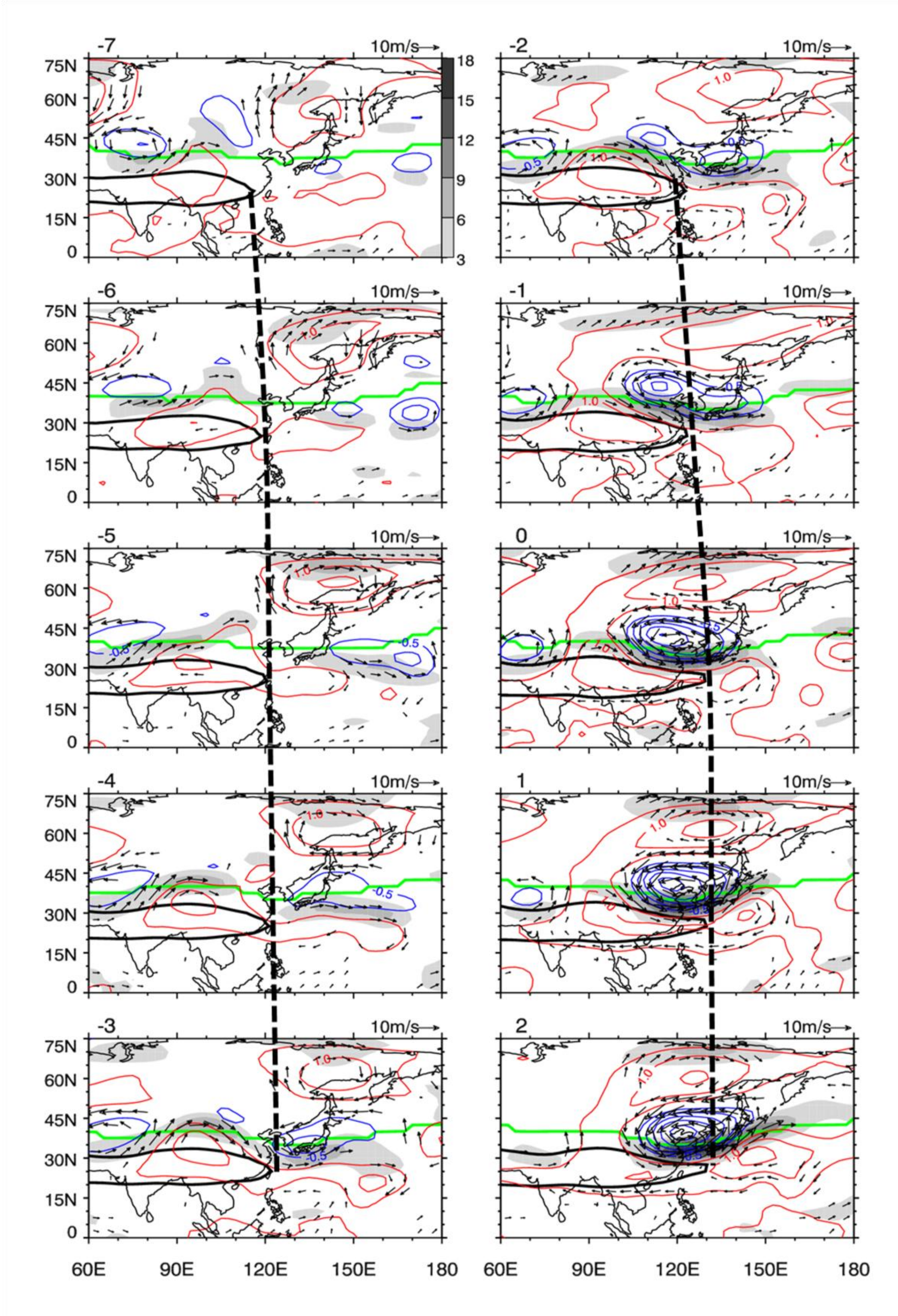

Figure 5. Composited 200 hPa horizontal wind anomaly (vectors, m/s) and normalized geopotential

height anomaly (contours, red for positive and blue for negative). The black solid line in each panel represents boundary of the South Asia High (12520gpm-contour). Only the vectors that are at least significant at the 0.05 level are shown. The shadings denote the zonal wind (U) speed anomaly, with interval 3m/s. The green bold line represents the jet axis. The number above each panel represents the same meaning of that in Figure 2. The black dashed lines portray the eastward propagation of the South Asia High

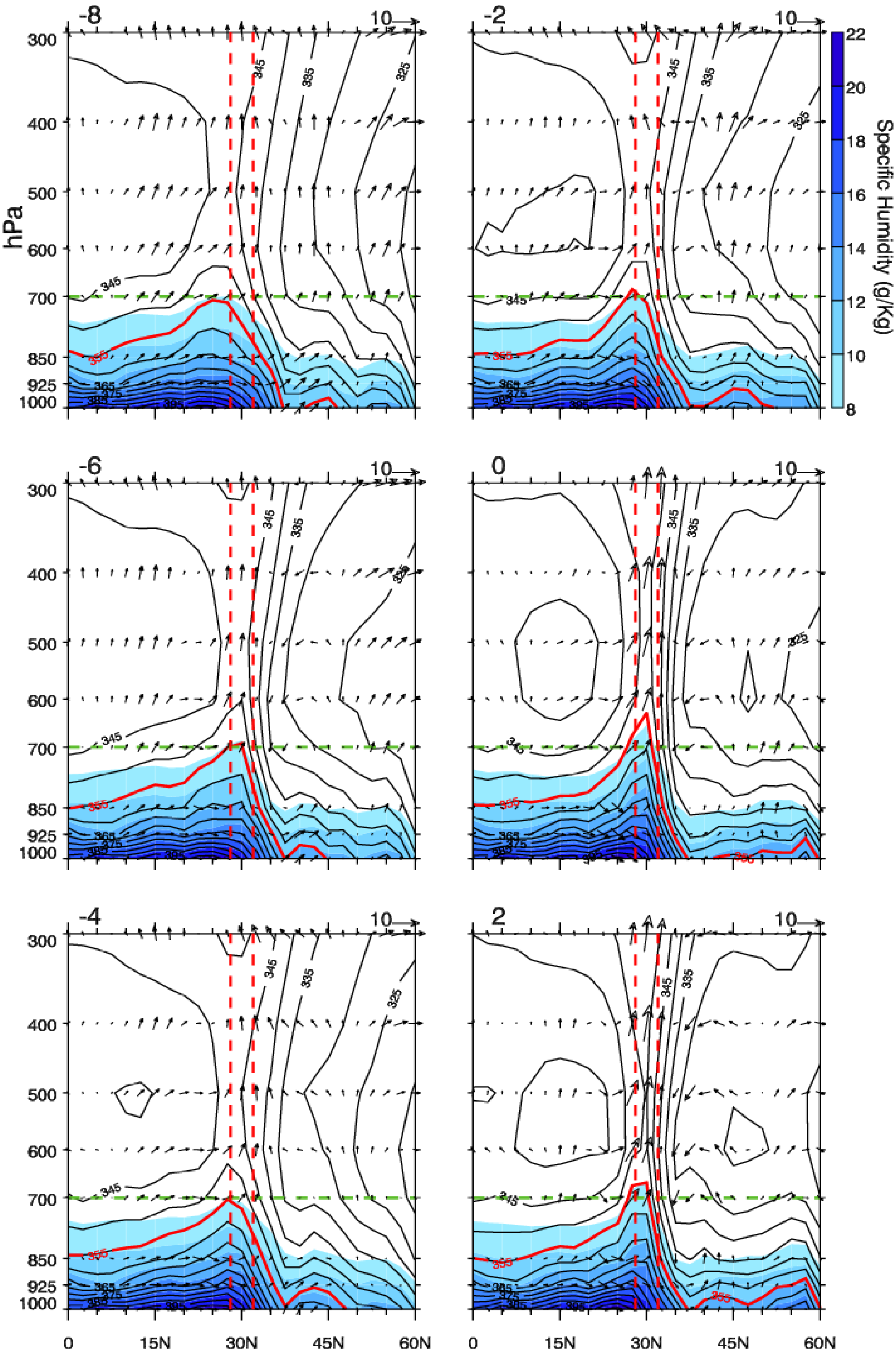

Figure 6. Composited latitude-height cross section (along 120 °E) of equivalent potential temperature (contour, every 5K), specific humidity (shading, every 2 g/kg) and wind (v-component, m/s;

-ω-component, 0.01 Pa/s). The red dashed line highlights the region within the YRV. The number above each panel represents the same meaning of that in Figure 2. The green dashed line labels the 700hPa isobaric surface, and 355K-contour of equivalent potential temperature is highlighted by red bold line.

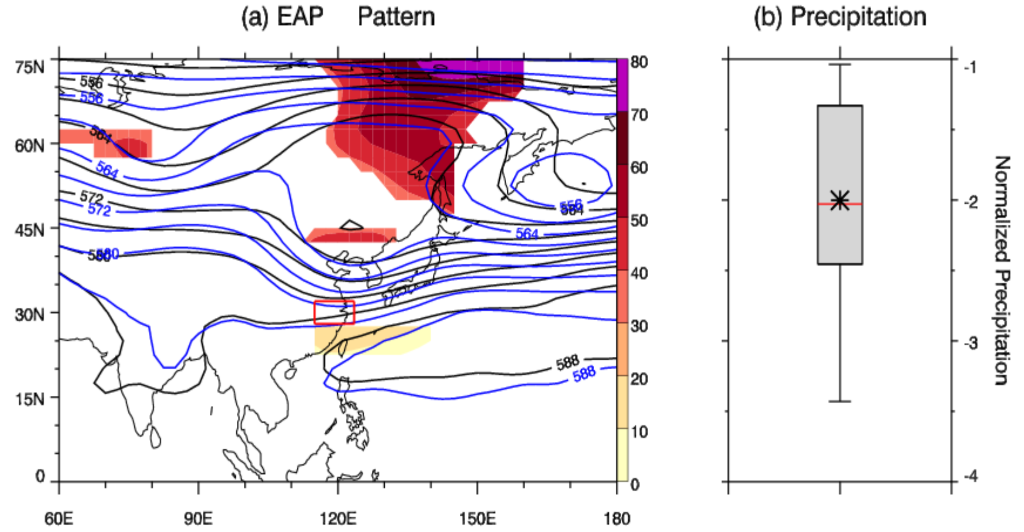

Figure 7. As in Figure 1, but for the EAP patterns that can't result in PEPEs in the YRV (typical dry EAP pattern). For (a), the black contours indicate the composited geopotential height in Figure 1 (typical wet EAP pattern) and the blue ones represent the composited geopotential height during dry EAP pattern (every 4 dagpm). The regions with significant differences (at least at the 0.05 level) between wet and dry (wet minus dry) are shaded. For (b), the sample size is 39 days as listed in Table 2.

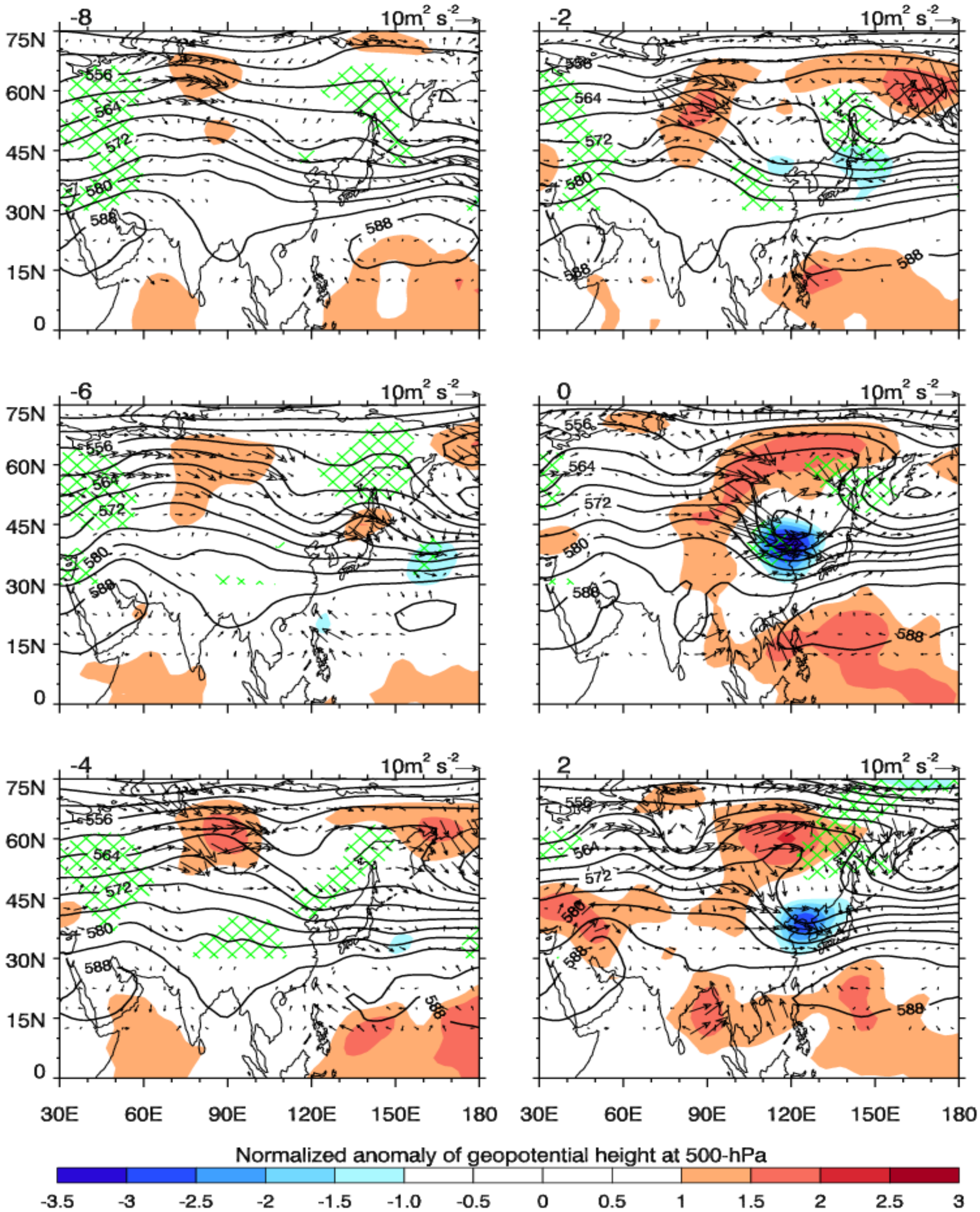

Figure 8. As in Figure 3, but for the EAP patterns that can't result in PEPEs in the YRV (typical dry EAP regimes). Only the significant anomalies (at least at the 0.05 level) of geopotential height with respect to climatology are shaded. The hatched lines indicate the significance of positive differences between wet and dry EAP regimes (wet minus dry) at the 0.05 level at least.

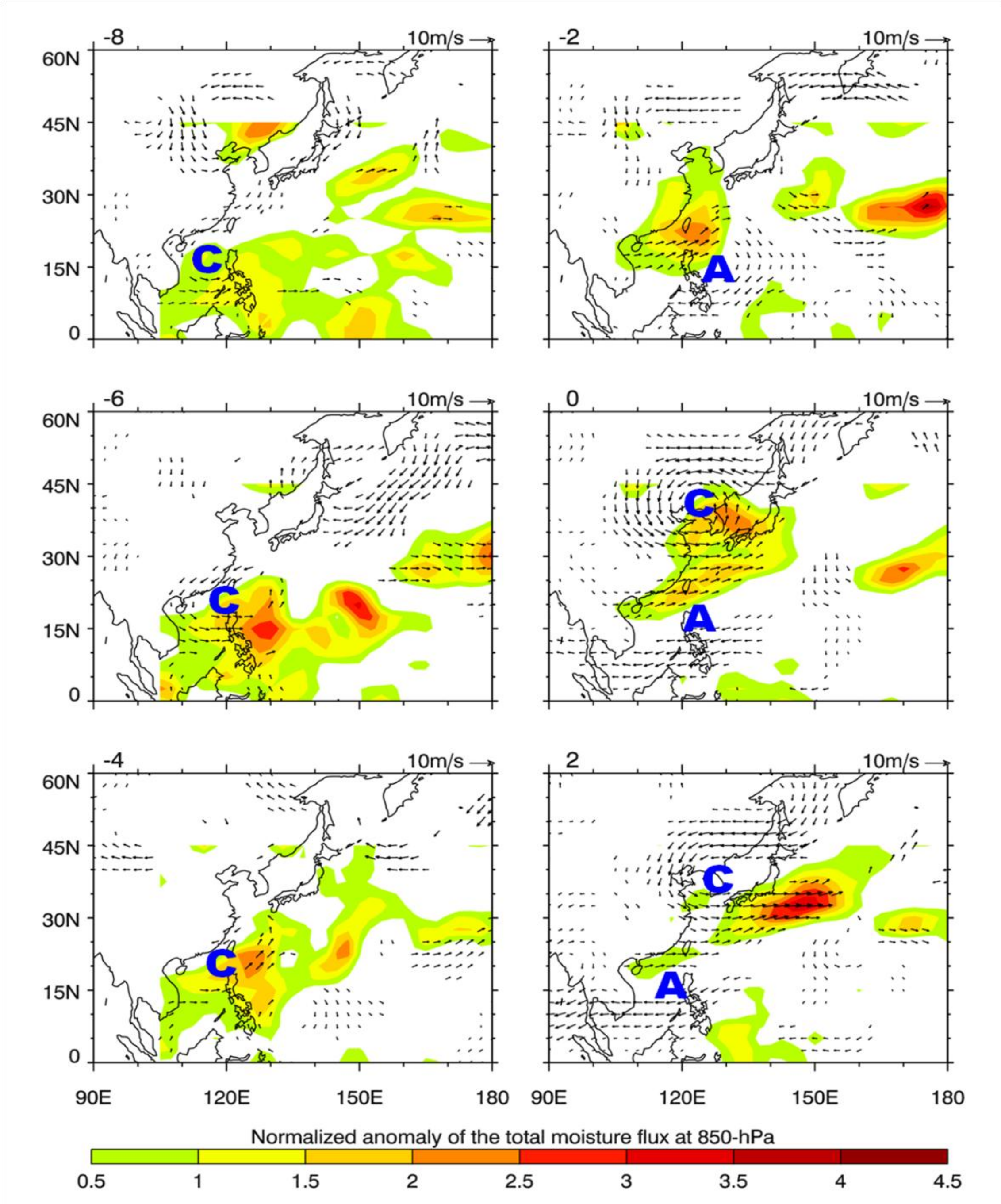

Figure 9. As in Figure 4, but for the EAP patterns that can't result in PEPEs in the YRV (typical dry EAP regimes)

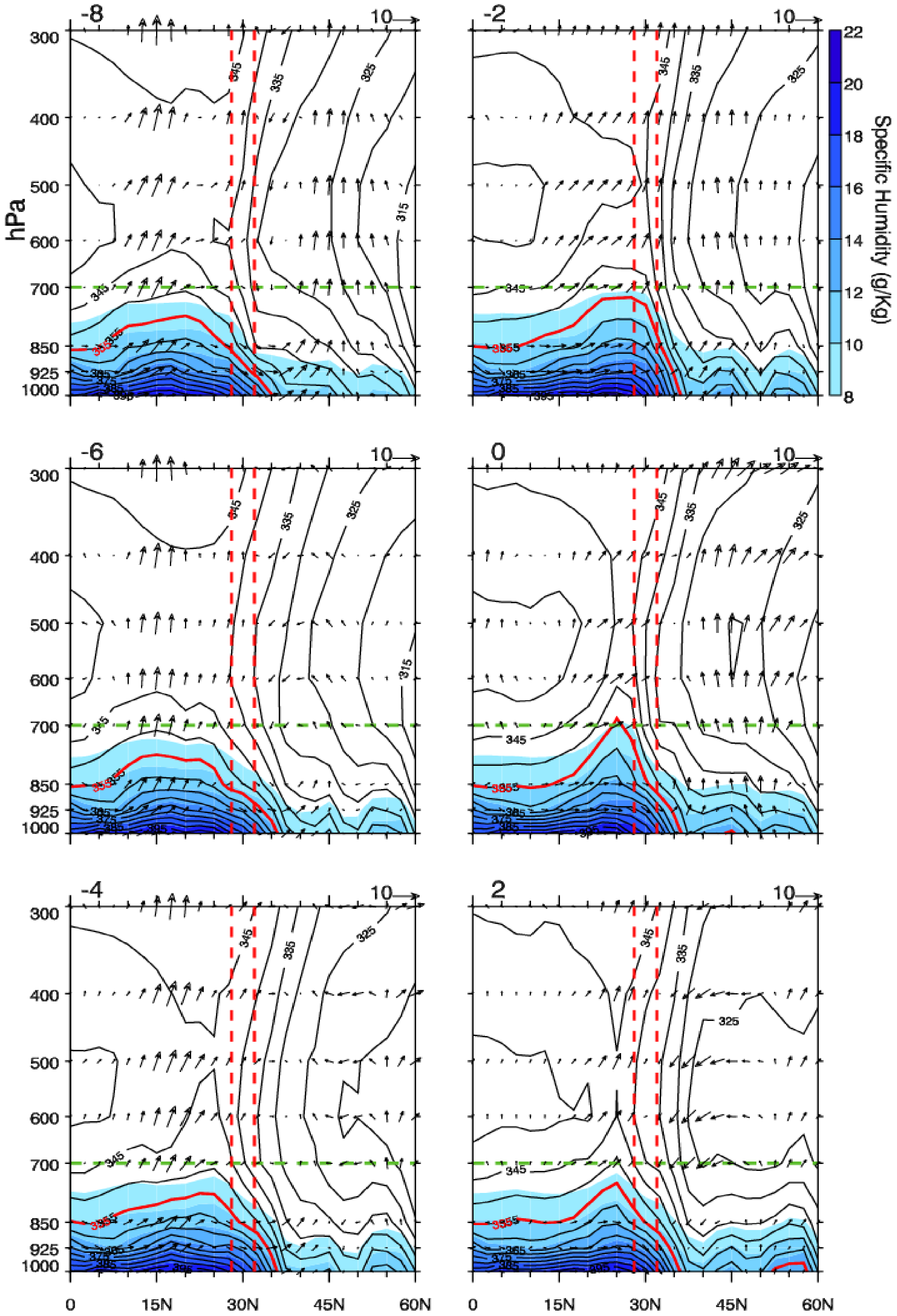

Figure 10. As in Figure 5, but for the EAP patterns that can't result in PEPEs in the YRV (typical dry EAP regimes)

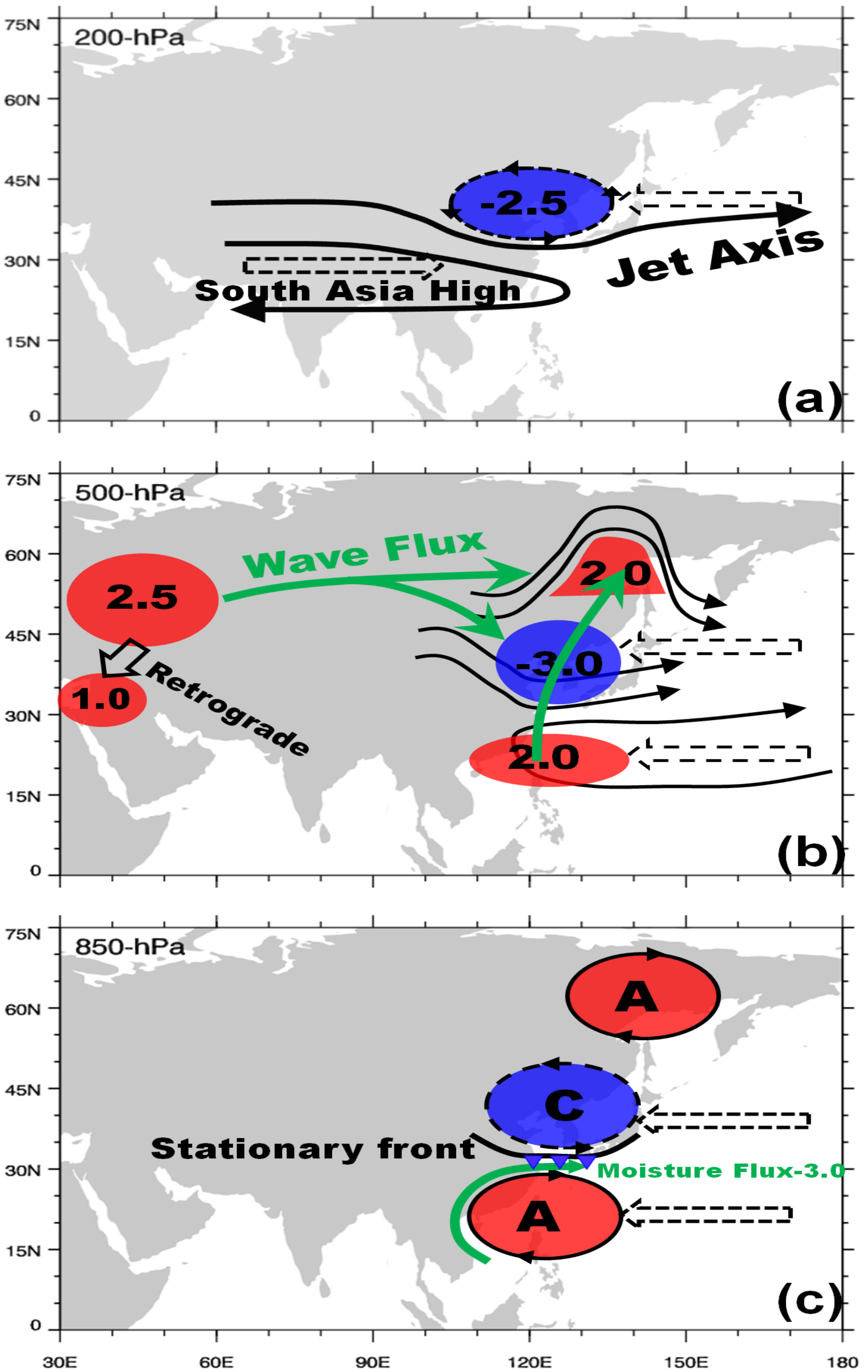

Figure 11. Schematics for precursor circulation features of typical EAP patterns responsible for

persistent extreme precipitation events in the YRV. The thick dashed blank arrows portray the propagating routines of these precursors. (a) is for 200 hPa, in which the black solid lines with arrowheads denote boundary of the South Asia High and westerly jet axis as labeled in the figure. (b) is for 500 hPa, in which the black solid lines with arrowheads stand for streamlines. The green arrows portray the wave fluxes propagation. The red and blue shadings denote positive anomalies and negative anomalies of geopotential height respectively, with the regional average normalized anomaly value at day -1 labeled on them. The shadings and values to the west of 60°E delineate the evolution of the western ridge. (c) is for 850 hPa. The red shadings and the letter 'A' represent the anomalous anticyclone. And blue shadings and the letter 'C' represent the anomalous cyclone. The green arrow represents the anomalously enhanced moisture flux, with its normalized anomaly of magnitude on day -1 (3 standard deviations above normal) labeled in text. The stationary front is presented as bold black lines with three blue triangles.